Rates of temperature change of airless landscapes and implications for thermal stress weathering

Jamie Molaro[1] and Shane Byrne[1]

Received 21 May 2012; revised 12 September 2012; accepted 14 September 2012; published 25 October 2012.

[1] Thermal stress weathering may play a role in the evolution of terrestrial-planet landscapes, particularly those without atmospheres, by contributing to rock breakdown, regolith production, and crater degradation. Damage occurs in the form of microscopic cracks that result from a thermal cycle or thermal shock. Terrestrial studies typically evaluate the efficacy of this process by measuring the rate of surface temperature change (dT/dt), using a damage threshold of 2 K/min. While the extent of this damage is unknown, we investigate its relative efficacy by modeling rates of temperature change on various airless surfaces. The magnitude of dT/dt values is primarily controlled by sunrise/set durations on quickly rotating bodies, such as Vesta, and by distance to the sun on slowly rotating bodies, such as Mercury. The strongest temperature shocks are experienced by highly sloped east- or west-facing surfaces. Hot thermal shocks ($dT/dt > 0$) tend to be stronger than cold shocks ($dT/dt < 0$), and on some bodies, daytime shadowing may produce higher dT/dt values than those caused by diurnal sunrise/set if the topography is optimally oriented. We find that high dT/dt values are not, however, always correlated with high temperature gradients within the rock. This adds to the ambiguity of the poorly understood damage threshold, warranting further research on the topic that goes beyond the simple 2 K/min criterion.

Citation: Molaro, J., and S. Byrne (2012), Rates of temperature change of airless landscapes and implications for thermal stress weathering, *J. Geophys. Res.*, *117*, E10011, doi:10.1029/2012JE004138.

1. Introduction

[2] Thermal stress weathering is the mechanical breakdown of rock from expansion and contraction caused by changes in temperature. Together with aeolian, fluvial, and chemical weathering, it plays a role in the evolution of Earth's landscapes, breaking down boulders, changing rock surfaces, and generating sediment. In most Earth environments, processes such as frost and chemical weathering dominate rock breakdown [e.g., *Wellman and Wilson*, 1965; *Cooke and Smalley*, 1968; *Hallet*, 2006]. However, in environments that lack significant amounts of water, thermal fracture may play a role in processes such as exfoliation, large crack formation, and granular disintegration [e.g., *Hall*, 1997, 1998, 1999; *Hall and Andre*, 2001, 2003; *Viles*, 2005; *McFadden et al.*, 2005; *McKay et al.*, 2009; *Sumner et al.*, 2004; *Eppes and Griffing*, 2010]. Thermal stress weathering may be significant on other inner solar system bodies, particularly those without atmospheres, by contributing to rock breakdown, regolith production, and crater degradation.

[3] Thermal fatigue is progressive, structural damage caused by thermal cycling from the diurnal cycle of the sun. Microscopic cracks are formed and enlarged each cycle due to thermal gradients and to mismatches in the thermal expansion coefficient in adjacent mineral grains. Terrestrial geomorphologists have debated for decades over the importance of this process. In a famous review paper, *Griggs* [1936] concluded that there was insufficient evidence to determine if the process operated at all. Another oft-cited study [*Blackwelder*, 1933] found that cracks could only be induced through thermal cycling if the heated samples were cooled with water. Many modern studies still argue that, while fatigue is an important and active process, the conditions necessary for it to operate without water simply do not exist on Earth [e. g. *Moores et al.*, 2008; *Sumner et al.*, 2007; *Viles*, 2005]. Laboratory studies of deteriorating marble and granite used as building materials show significant strain when subjected to thermal cycling [e.g., *Koch and Siegesmund*, 2004; *Siegesmund et al.*, 2008; *Gómez-Heras et al.*, 2006], and some emphasize that moisture is not required to cause damage in materials composed of minerals with anisotropic thermal expansion coefficients [e. g. *Luque et al.*, 2011]. *McFadden et al.* [2005] and *Eppes et al.* [2010] found that fractures caused by thermal fatigue in deserts in the southwestern United States, Mongolia, and Australia were found to be predominantly N-S in orientation, suggesting that they formed due to a N-S stress field formed in a boulder from the sun moving E-W across the sky. This may be similar on

[1]Lunar and Planetary Laboratory, University of Arizona, Tucson, Arizona, USA.

Corresponding author: J. Molaro, Lunar and Planetary Laboratory, University of Arizona, 1629 E. University Blvd., Tucson, AZ 85721, USA. (jmolaro@gmail.com)

0148-0227/12/2012JE004138

other bodies as well, assuming that the thermal stresses are high enough to form fractures at all.

[4] Thermal shock has been treated differently than fatigue in the geomorphology literature, and is characterized by formation of a macroscopic failure plane in response to a rapid change in temperature. The rapid change in surface temperature induces a strong spatial thermal gradient within the rock that can cause immediate catastrophic failure [*Lu and Fleck*, 1998]. This is often observed in glass, ceramics, or building materials, but has also been seen to cause rock failure in extreme environments such as Antarctica or the Atacama Desert. Many studies consider rates of surface temperature change when studying this process, as it is more easily recorded (in the field) or controlled (in the lab) than the spatial temperature gradient. *Richter and Simmons* [1974] found experimentally that heating igneous rocks at rates >2 K/min generated immediate macroscopic cracks in an Earth environment. However, it is ultimately the spatial gradient that causes damage. The relationship between the temporal and spatial temperature gradients has not been well studied in the past, nor is a threshold for the spatial gradient required to cause damage known. Instead, the result found by Richter and Simmons has been misused in that it is now typically considered a requirement for thermally induced damage [e.g., *Hall*, 1999; *Viles et al.*, 2010]. Studies using this threshold typically acknowledge its deficiencies, but little work has yet been done to rectify them. Simple heat conduction models of the energy exchange between a rock and the environment can accurately reproduce temperature changes at and near an idealized surface, especially at larger spatiotemporal scales [*Vasavada et al.*, 1999; *Molaro and McKay*, 2010; *Gunzburger and Merrien-Soukatchoff*, 2011]. However, due to natural variation in diurnal and annual thermal forcing, as well as the complexity of the rock structure at small scales, subsurface stress fields induced by surface temperature variations are extremely complex, making use of a general, constant threshold value rather uninformative. Although of questionable relevance, we continue to compare our results to this 2 K/min criterion. Further research is needed to understand what thermal conditions are actually required to cause damage in different types of rocks and environments.

[5] The distinction between fatigue and shock on a microphysical level is somewhat ambiguous, as failure in both cases results from the coalescence of microcracks. Monitoring of crack formation with acoustic emission equipment has shown that, during fatigue experiments, microcracks multiply and propagate before linking up and causing macroscopic catastrophic failure of the sample [*Jansen et al.*, 1993]. The primary distinction between fatigue and shock is then how quickly this occurs, as all rocks that appear to "suddenly" fail have already been thermally fatigued to different extents. In addition, *McKay et al.* [2009] and *Molaro and McKay* [2010] have shown that small scale, high frequency temperature fluctuations caused by wind eddies may cause enough thermal stress to break down rock surfaces. Rapidly fluctuating, high thermal stresses at the grain scale could produce what would be considered thermal shock at the grain scale, but which may be interpreted as fatigue when observing macroscopic scales. There is, as yet, a lack of understanding of the relationship between the scale of operation and the scale of observation of thermal stress in rocks, and of the implications of that relationship for rock breakdown. In this study, we consider thermal stresses from illumination and shadowing at time scales shorter than the diurnal cycle to be thermal shock, in the sense that the temperature changes observed are rapid. Likely stresses in these cases would be enough to cause microfractures to form or lengthen, but not to cause immediate catastrophic failure at macroscopic scales, making breakdown a slow and progressive process similar to what is thought of as fatigue.

[6] While the damage caused by this process is yet unknown, looking at rates of temperature change on different bodies will indicate how susceptible to this process they may be, even if only in a relative sense. Airless bodies provide perhaps the environment most conducive to thermal weathering, as the surface rocks can heat and cool at greater rates and over a greater temperature range. The presence of an atmosphere dampens the heating and cooling rates experienced by a rock surface through sensible heat exchange and radiative effects. During heating, the atmosphere's opacity limits the amount of solar flux available at ground level to heat the rock's surface. During cooling, the atmosphere emits long wavelength radiation, providing a source of heat even while the rock is shaded. Thus, on bodies that lack atmospheres, thermal shocks from sudden shadowing or illumination on a rock surface may yield thermal stresses great enough to cause permanent damage. This effect would be additive to the damage these bodies experience due to fatigue. To a certain extent, fractures formed daily from thermal shocks is itself thermal fatigue, but since the distinction between the two is not yet well defined we will, for the moment, refer to them as two separate processes.

[7] Bodies that are closest to the sun and have the longest days experience the highest diurnal temperature variation. The thermal stress associated with a periodic temperature variation is proportional to the amplitude of that temperature variation (ΔT). In reality, surfaces are compositionally heterogeneous and pre-existing fractures concentrate the stress field at crack tips, so these stresses represent only a lower limit. Bodies such as many asteroids have fast rotation rates. This increases the frequency of thermal cycling, but also makes their surfaces even more susceptible to high rates of temperature change. This suggests that thermal stress weathering both from fatigue and from shocks may be relevant on these surfaces. *Dombard et al.* [2010] suggested that thermal stress weathering is responsible for smooth ponds of material found on the asteroid Eros, and *Viles et al.* [2010] found that only modest temperature cycles are required to cause breakdown of boulders on Mars. In this study, we will focus on quantifying thermal shocks by using a thermal conduction model to examine rates of temperature change on airless, rocky surfaces in the inner solar system.

2. Thermal Model

[8] We use a simple, one-dimensional heat conduction model [e. g. *Vasavada et al.*, 1999; *Gunzburger and Merrien-Soukatchoff*, 2011] of a unit area surface on the Moon, Mercury, and Vesta to calculate the maximum rates of temperature change (dT/dt) and explore optimal parameters for rapid temperature changes. The heat conduction equation is:

$$\rho c_p \frac{dt}{dt} = k \frac{d^2 T}{dz^2} \tag{1}$$

where ρ is the rock density, c_p is the specific heat, k is the thermal conductivity, and z is depth into the rock interior. Values for these properties, shown in Table A1, are typical of basalt and taken to be constant, as this study only considers bedrock surfaces. Since a variety of rocks with differing properties occur on planetary surfaces, a sensitivity study of the model was done to determine the relative dependence of model results on each property. This study, discussed in Appendix A, found that rock property values (especially thermal conductivity) can influence the strength of dT/dt values by up to a factor of two.

[9] The boundary conditions at the rock surface and bottom (z = D) are given by:

$$S - L + k\left.\frac{dT}{dz}\right|_{z=0} = 0 \tag{2}$$

$$Q - k\left.\frac{dT}{dz}\right|_{z=D} = 0 \tag{3}$$

where L is the emitted longwave radiation from the surface to open sky and S is the absorbed shortwave radiation from the sun. The constant heat flux at the bottom boundary layer is determined by the average heat production of the planet:

$$Q = r\rho_{ave}\frac{H}{3} \tag{4}$$

where r is average planetary radius, ρ_{ave} is the average planetary density, and H is a chondritic heat production rate of 5.5×10^{-12} W/Kg. The solar flux hitting the surface is calculated from the following equations for the cosine of the incidence angle on flat ground (i_f) and on sloped ground (i_s):

$$\cos(i_f) = \sin(\alpha)\sin(\beta) + \cos(\alpha)\cos(\beta)\cos(\delta) \tag{5}$$

$$\cos(i_s) = \cos(i_f)\cos(\theta) + \sin(i_f)\sin(\theta)\cos(\phi - \varphi) \tag{6}$$

where α is the latitude, β is the solar declination, δ is the hour angle, θ is the slope, and ϕ is the aspect angle. The slope is measured as the angle between the surface normal and vertical. The aspect angle is the orientation of the surface measured as degrees East of North. φ is the solar azimuth, given by:

$$\cos(\varphi) = \frac{\sin(\beta) - \sin(\alpha)\cos(i_f)}{\cos(\alpha)\sin(i_f)} \tag{7}$$

Surfaces with slopes ≥40° are composed entirely of bedrock, while those with slopes <40° are generally covered with unconsolidated regolith. Any bedrock surface with a regolith cover is insulated from thermal shocks of any interest, thus results discussed in the following sections do not report on surfaces below 40°. We will examine thermal stresses in regolith grains in future work.

[10] The total solar flux absorbed by the surface is then calculated:

$$S = (1 - A)\frac{S_o}{R^2}\cos(i_s) \tag{8}$$

where S_o is the solar constant, A is the surface albedo, and R is the body's solar distance. The longwave radiation emitted from the surface to open sky is slope-dependent and calculated with:

$$L = \sigma\varepsilon T_o^4 \cos^2(\theta/2) \tag{9}$$

where σ is the Stefan-Boltzmann constant, ε is the surface emissivity, and T_o is the surface temperature. Equation (9) assumes the slope is surrounded by an infinite flat plane of equal temperature. This is an approximation, however using a two temperature model was found to have a negligible effect on peak dT/dt values. More information on this effect and on other model complexities is available in Appendix A. The temperature of each layer is calculated using standard explicit finite difference methods to solve equations (1)–(4) throughout an insolation cycle. The highest magnitude dT/dt values calculated for a complete insolation cycle, with a given set of parameters, are recorded. These results allow us to identify optimal slopes and orientations that cause large thermal shocks, and compare dT/dt values to the canonical threshold of 2 K/min. Values for i_f, R, β, δ, and φ, used in equations (5)–(8), were supplied by the NAIF SPICE toolkit [*Acton*, 1996]. Initial conditions for the Moon and Mercury were taken from previous thermal models [*Vasavada et al.*, 1999], and on all bodies, the model was run for several diurnal cycles before any dT/dt values were recorded. For model runs on the Moon, the longitude is arbitrary. The longitude for Mercury was set so that noon occurs at perihelion (a "hot spot"), giving surfaces the hottest daytime temperatures and the shortest sunset durations. Vesta is a triaxial body and thus has a preferred longitude for maximum solar heating. This effect on dT/dt values is small however, and so for simplicity we chose a longitude of 0°. In contrast to the Moon and Mercury, Vesta has a large obliquity (~26°) and so season affects surface temperature. Vesta's fast rotation (leading to sunsets as short as 12 s) also demands a short model timestep to accurately quantify peak dT/dt. It was computationally prohibitive to model several Vesta years at such a short timestep for the large number of latitude/slope/aspect combinations we investigated. Instead, we first ran our model for several annual cycles at lower temporal resolution in order to determine the annual-average surface temperature and which day of Vesta's year produced the strongest thermal shocks at each latitude. Most of these days (referred to as peak days) occurred during peak annual solar flux. Peak solar fluxes in the northern and southern hemispheres occur relatively close together in orbit. In general, peak days all occurred near perihelion, regardless of latitude or season. We then ran our model at higher temporal resolution for several Vesta days at this optimal time of year and used these results to record peak positive and negative dT/dt. We used the annual-average temperatures at that latitude as initial conditions to this high temporal resolution model (although the peak dT/dts recorded were found to be insensitive to initial conditions).

[11] Both the time step and layer thickness in the model were made small enough that varying them produces no appreciable change in the magnitude of the results. See Appendix A for more detail on how model parameters were chosen. The strongest shocks occur at the surface, and peak dT/dt values experienced by each layer are damped with depth, as expected

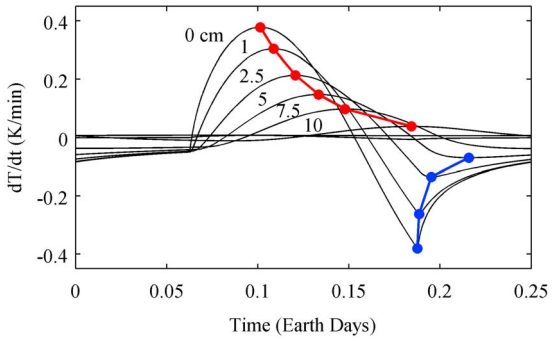

Figure 1. The black lines show dT/dt values over time of a flat, equatorial surface and several subsurface layers for an arbitrary body with a solar day length of 0.25 Earth days, at 1 AU from the sun. The red line is peak positive dT/dt values at each layer, and the blue, peak negative.

(Figure 1). The effective damping depth of the shock is also not affected by variations in layer thickness or time step. Many layers may experience dT/dt values greater than a given threshold. Since the implications of these shocks on how much damage may be occurring is yet unknown, we refer to thermal shocks in this paper very generally as events happening at or near (within 0.5 m of) the rock surface.

2.1. Varying Slope and Aspect on the Moon, Mercury and Vesta

[12] In this model (referred to the "slope/aspect model"), we focused on varying the latitude, slope and aspect angles of surfaces on the Moon, Mercury, and Vesta. Latitudes of 0°, 45°, and 85° were used for each body. In spite of Vesta's obliquity and triaxial shape, peak dT/dt values in northern and southern latitudes are nearly identical. In each model run, the slope was varied from 0° to 90°.

[13] The finite size of the solar disk means that sunrises and sunsets have some duration determined by the body's rotation rate and the sun's angular radius, and thus changes in solar flux during these events are gradual. The minimum sunrise/set durations for surfaces on the Moon, Mercury, and Vesta are ~1 h, ~8 h, and ~12 s, respectively. Sunrise/set durations increase with latitude as sunrises/sets become more oblique, and with longitude on bodies like Mercury with complex spin-orbit effects. Seasonal effects on Vesta due to its large obliquity also cause sunrises/sets to become oblique, even on equatorial surfaces. This variation in the amount of time it takes for these events to occur is important to account for, as it affects how quickly the surface will be able to heat up or cool off as a result. See Appendix A for a description of how the size of the solar disk is accounted for in these and the following cases. A sufficiently small time step was used in all cases to ensure many steps occurred during these events.

[14] To simulate the effect of a shadow caused by surrounding topography sweeping across the surface during the day, some model runs include an artificial shadowing event. In these cases, we placed a shadow over the surface for a period of time appropriate to record the strongest dT/dt values (see Appendix A). Theoretically, topographically induced shadows can occur at any time of day. We placed our artificial shadows during morning (8 A.M.) and afternoon (3 P.M.) on each body. We will use the terms morning shadowing and afternoon shadowing to refer to these events (or daytime shadowing, if referring to both), as distinguished from sunrise and sunset. It will be necessary at some points to discuss a local sunrise/set that occurs as a result of this shadowing. For clarity, we will refer to these as artificial sunrises/sets. It is relevant to note that, at the equator, this type of topographic shadowing cannot occur on bodies with zero obliquity. We chose to include the dT/dt values for equatorial artificial shadowing on the Moon and Mercury in spite of this fact to provide a comparison to higher latitudes. In addition to shadows that occur during the day, shadows that delay sunrise (surfaces where the sun rises later due to shadowing topography) may also produce strong shocks. These surfaces could have shallower slopes, which are more common and widespread on planetary surfaces. Since lower slopes are more likely to be covered by regolith it is difficult to tell how important this effect may be.

[15] It is extremely important to account for the size of the solar disk all cases. An example of an artificial shadow where the solar disk is considered predicts dT/dt values of ~0.5 K/min (Figure 2c) for Mercury. Treating the sun as a point source leads to much higher (and erroneous) predictions of dT/dt values ~50 K/min (Figure 2d). Comparing hard and soft edged shadows on the Moon and Vesta shows similar effects, with dT/dt values being affected by about 2 orders of magnitude. Most studies do not compare hard or soft edged shadows, as it has little effect on the overall surface temperature. As we have shown, however, it does have a large effect on the peak rates of temperature change and is important to consider. This also indicates that a body's rotation rate and distance from the sun will likely play a large role in the effectiveness of thermal weathering on its surface, since the smaller the angular size of the solar disk, the more hard-edged a shadow will be and the faster the body rotates, the shorter the duration that surface experiences this shadow edge.

2.2. Varying Length of Insolation Cycle and Distance to Sun on Arbitrary Bodies

[16] A second, similar model (referred to as the "day length model") was used to explore the strength of thermal shocks as a function of solar day length and distance to the sun. In this case, latitude, obliquity, and orbital eccentricity were set to zero, therefore removing any seasonal effects. The length of the solar day was varied from 0 to 30 Earth days, and the distance to the sun from 0 to 2.5 AU. Results from these models allow us to see which bodies in the inner solar system (e.g., among the near Earth asteroids) may be most affected by thermal stress weathering. Based on results of our slope/aspect investigation, we chose for this model a surface slope of 65° at two aspect angles, 90° and 270°.

3. Model Results

3.1. Slope/Aspect Model

[17] Here we investigate where we should expect thermal stress weathering to be most effective on airless bodies. The thermal shocks recorded are separated into hot (compressional) shocks, where dT/dt is positive, and cold (tensional) shocks, where dT/dt is negative. Figure 3 shows contour plots of greatest magnitude hot and cold shocks, respectively, on the Moon's surface at varying latitudes. The strongest hot shocks occur on highly sloped, east-facing surfaces that

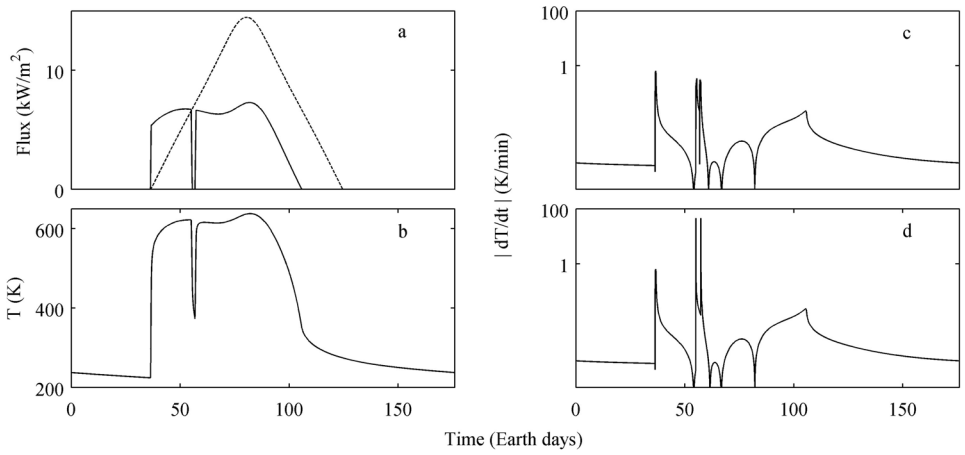

Figure 2. (a) The solar flux incident upon a surface at the equator on Mercury with a slope of 60° and an aspect of 80°, with corresponding (b) surface temperature and rate of change in temperature caused by a (c) soft-edged and (d) hard-edged shadow. Both Figures 2c and 2d are semi-log plots. The dashed line in Figure 2a is the solar flux that would be incident on flat ground. In this test, an artificial shadow was introduced in the morning (at t ∼ 60 Earth Days).

warm quickly when the sun rises. Similarly, the strongest cold shocks occur on highly sloped, west-facing surfaces that remain hot until the sun sets, after which they cool quickly. We will refer to these two geometries as optimal geometries, in that they experience significantly higher thermal shocks than non-optimal geometries. The strength of the shocks decreases with increasing latitude because the sunrises/sets become more oblique and so occur more slowly. Hot shocks at all latitudes are equal or stronger than cold shocks on both the Moon and Mercury, where the effects are more dramatic due to its proximity to the sun. Note that this does not necessarily suggest that cold shocks cause less damage, as the relationship between dT/dt and incurred damage is still unknown. Hot shocks on Mercury's surface are stronger than those same cases for the Moon, though most of its cold shocks are weaker due to its lengthier sunsets. The highest magnitude dT/dt values from these plots and those discussed in the remainder of this section are listed in Table 1.

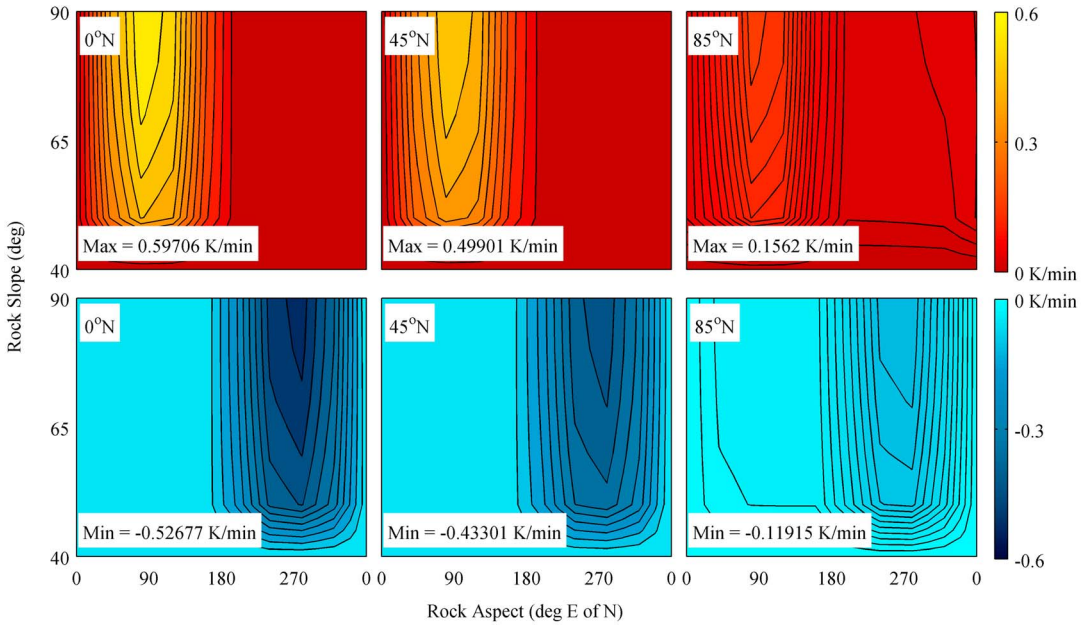

Figure 3. Contour plots of (top) maximum and (bottom) minimum recorded dT/dt values as functions of rock slope, aspect, and latitude on the Moon. Contour lines are every −0.05 K/min for latitudes 0° and 45°, and −0.01 K/min for latitude 85°. The max and min values listed on the plots are the largest magnitude dT/dt values found in each panel.

Table 1. Peak dT/dt Values[a]

Body	Case		Peak dT/dt (K/min) Latitude 0	Latitude 45	Latitude 85
Moon	No Shadow	Hot	0.597	0.499	0.156
		Cold	−0.526	−0.433	−0.119
	Morning Shadow	Hot	0.597	0.539	0.540
		Cold	−0.532	−0.537	−0.547
	Afternoon Shadow	Hot	0.597	0.518	0.528
		Cold	−0.527	−0.529	−0.537
Mercury	No Shadow	Hot	0.784	0.623	0.228
		Cold	−0.415	−0.412	−0.221
	Morning Shadow	Hot	0.785	0.624	0.381
		Cold	−0.415	−0.412	−0.395
	Afternoon Shadow	Hot	0.784	0.623	0.351
		Cold	−0.416	−0.412	−0.325
Vesta	No Shadow	Hot	2.141	1.863	0.603
		Cold	−2.059	−1.427	−0.097
	Morning Shadow	Hot	6.149	5.396	5.123
		Cold	−7.289	−5.522	−6.259
	Afternoon Shadow	Hot	4.361	3.761	3.569
		Cold	−3.570	−2.383	−2.692

[a]This table shows peak dT/dt values produced in cases with no artificial shadowing, morning shadowing, and afternoon shadowing on each body. The peak values are strongest shocks out of the entire range of slopes and aspects in that model run.

[18] In cases where an artificial shadow is introduced during the day, the results show different trends. The range of peak dT/dt values across all three latitudes is much smaller than cases without shadowing and the latitude dependence is not always preserved. This is because the topography casting the shadow is assumed to be oriented normal to the sun's path across the sky (what we term horizon-normal), yielding the fastest possible artificial sunrises/sets, equivalent to the natural sunrises/sets at the equator during equinox. So shadowing hardly affects maximum dT/dt values at the equator, but can produce much higher values at higher latitudes. Figure 4 shows hot and cold shocks, respectively, for morning shadowing, and Figure 5 for afternoon shadowing for a surface on the Moon. While this represents an ideal case rather than perhaps a realistic one, it demonstrates that shadowing does not produce significantly stronger shocks than sunrise/set. Slightly stronger hot and cold shocks are produced by the morning shadow than by the afternoon shadow, but the effect is small since the incident solar flux at the time each shadow occurs is similar. Both Figures 4 and 5 include data for dT/dts caused by sunrises/sets as well as from daytime shadowing, causing two sets of maxima to be visible. The maxima caused by daytime shadowing occur on lower slopes than those from sunrises/sets. Peak dT/dt values from daytime shadowing occur on slopes receiving the highest solar fluxes at the time of shadowing; in this case, slopes of 50° at the equator and higher toward the pole.

[19] On Mercury's surface, the introduction of either a morning or afternoon shadow has little effect on the peak dT/dt values due to the fact that Mercury rotates slowly and sees a large solar diameter, making even a "sudden" shadowing event take a relatively long time to occur (even at the pole dT/dt values for hot shocks only increased by a maximum of ∼0.15 K/min). Cold shocks once again are weaker and have less variation with latitude than hot shocks. The values for hot and cold shocks of morning versus afternoon shadows are comparable in strength, though again slightly stronger for the former.

[20] Vesta cases differ quite significantly from the Moon and Mercury. Due to its short sunrise/set duration, shadowing and illumination occur rapidly, causing high rates of temperature change, in spite of receiving a much lower incident solar flux. All hot and cold shocks experienced by Vesta's surfaces are much stronger than on the Moon or Mercury.

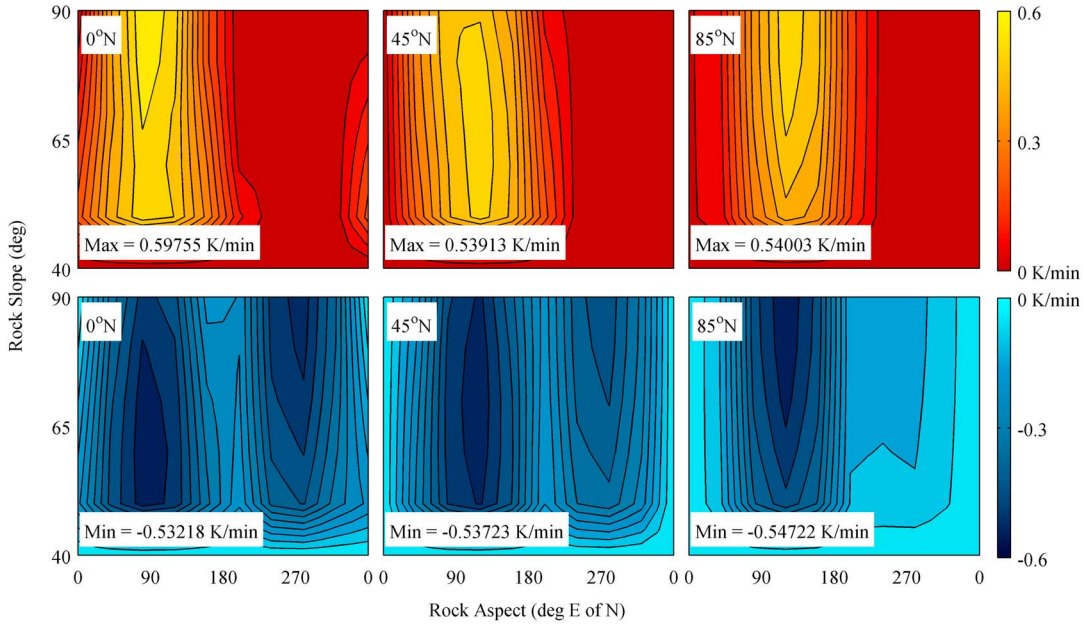

Figure 4. Panels are the same as Figure 3 for the case where an artificial shadow is emplaced on the surface in the morning.

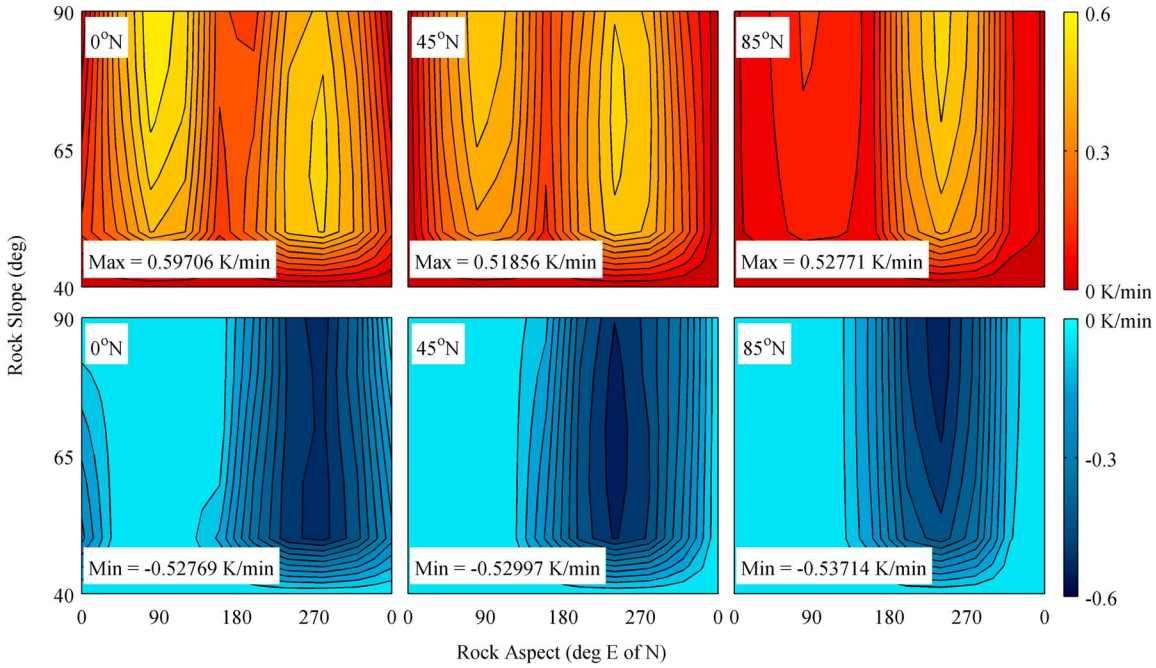

Figure 5. Panels are the same as Figure 3 for the case where an artificial shadow is emplaced on the surface in the afternoon.

Peak dT/dt values at the equator are comparable to the canonical threshold for damage. In cases with daytime shadowing, both hot and cold shocks are strengthened significantly. The largest increase in shock strength occurs at the poles, again due to the imposed shadow being horizon-normal, where dT/dt values were already much lower than at the equator and midlatitudes. All shocks that occur as a result of morning shadowing are stronger than those caused by afternoon shadowing, possibly due to interaction with heat stored in the subsurface at different times of day.

[21] As discussed in the introduction, rapid changes in temperature set up spatial temperature gradients ($dT/dz = (L - S)/k$, from equation (2)) inside rock surfaces, which ultimately cause damage. While there is no accepted threshold for the dT/dz required to form or propagate cracks, it is interesting to compare dT/dt values to dT/dz values in our model results to gain a better understanding of their relationship. Figure 6 shows the peak hot and cold dT/dt contour plots for each body at the equator, overlain by contour lines of peak dT/dz. In the model, z increases in the downward or subsurface direction, i.e., dT/dz is negative when heating from the top is occurring. For this reason, the hot shocks are overlain by peak minimum dT/dz values, and the cold shocks by peak maximum dT/dz. Values are measured between the surface and the center of the first model layer. The strongest dT/dz values occur at the optimal geometries (morning heating and afternoon cooling) with a second (weaker) set of maxima that occur at non-optimal geometries. Due to the extreme temperatures of the surface, the magnitude of dT/dz values on Mercury reaches up to ~2000 K/m. In contrast, even though Vesta's surface experiences the highest dT/dt values of the three bodies, it yields dT/dz values with magnitudes of only ~110 K/m or lower.

3.2. Day Length Model

[22] The previous results indicate where and when on an airless body thermal weathering may be most effective. To determine on which bodies it might be most effective, we can look at the highest magnitude dT/dt values found on a body's surface (known from section 3.1 to be at the equator) as a function of length of insolation cycle and semi-major axis. Figure 7 shows hot shocks on east facing slopes (Figure 7, top) and cold shocks on west facing slopes (Figure 7, bottom) of 65°. While vertical slope faces show the highest dT/dt values, they are uncommon, thus the slope of 65° was chosen as a compromise between optimal and more common surfaces. Note that, while the locations of the bodies indicated on the plot are accurate, this dT/dt calculation does not account for obliquity or orbital eccentricity.

[23] Similar to the results discussed in the previous section, optimal geometries show strong thermal shocks and a large area of parameter space with $|dT/dt| > 2$ K/min. Both hot and cold shocks in these cases scale similarly with increasing distance from the sun, but they differ when increasing the length of the solar day. Even the optimal case for cold shocks shows that $|dT/dt|$ values exceeding 2 K/min are limited to bodies with rotation periods less than ~25 Earth days, whereas the limit for hot shocks extends far beyond that. This is due to the fact that bodies with long cycles cool dramatically at night, allowing for strong hot shocks when the sun rises, whereas during the day the maximum surface temperature is limited by the albedo and increasingly efficient thermal emission of the bedrock and thus there is an upper limit to how strong cold shocks can be during sunset.

[24] In addition, 2 K/min is exceeded by many bodies with fast rotation rates that are relatively distant from the sun, such as Vesta. As previously discussed, quickly rotating

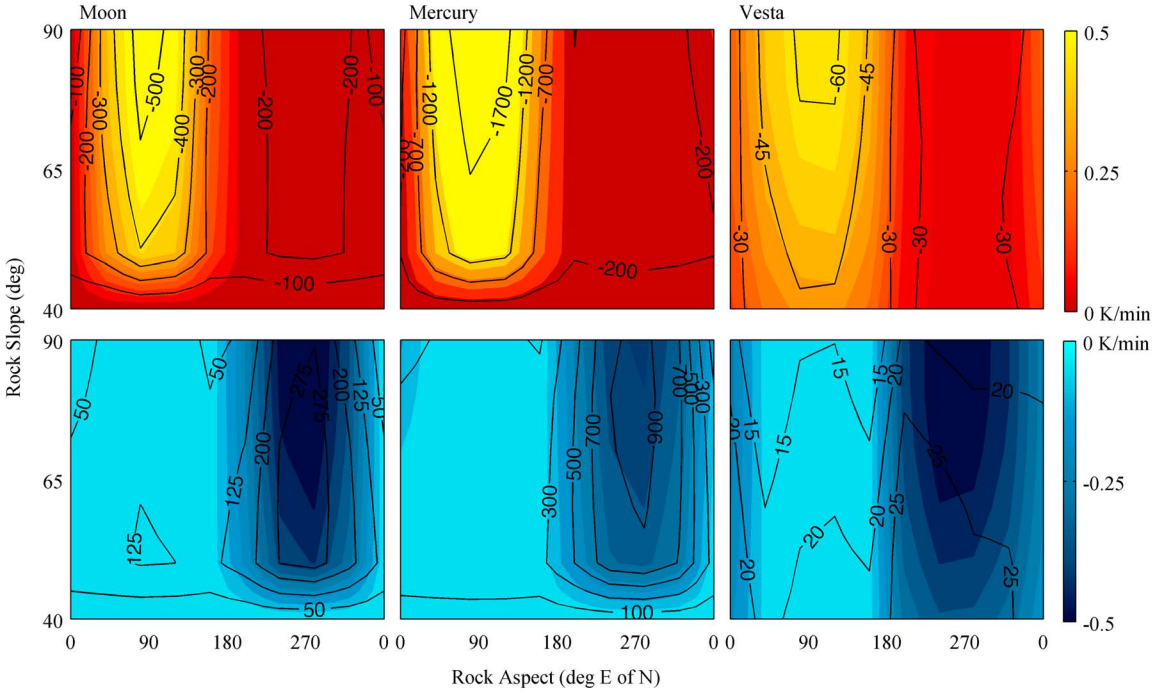

Figure 6. Contour plots of maximum and minimum dT/dt values (color) for equatorial surfaces on the Moon, Mercury, and Vesta as functions of slope and aspect angle, overlain by contours of corresponding dT/ dz magnitudes (black lines). The color axis for Vesta is normalized to those of Mercury and the Moon, with max/min values of +/−0.5 K/min. On the Moon, the strongest cold shock is −0.5 K/min, with a spatial gradient of 543 K/m, and the strongest hot shock is 0.6 K/min with a spatial gradient of −313 K/m. On Mercury the strongest cold shock is −0.4 K/min, with a spatial gradient of 972 K/m, and the strongest hot shock is 0.8 K/min with a spatial gradient of −2042 K/m. On Vesta the strongest cold shock is −2 K/min, with a spatial gradient of 112 K/m, and the strongest hot shock is 2 K/min with a spatial gradient of −110 K/m.

bodies produce the highest rates of temperature change, so bodies with the largest dT/dt values are also the bodies with the highest cycling rate, suggesting that thermal stress weathering may modify landscape at a much faster rate. However, since high dT/dt values do not always correlate directly to high dT/dz values it is uncertain to what extent surface dT/dt is a reliable predictor of thermal damage.

[25] This model can also be used to explore why the duration of the sunrise/set is so important in determining maximum dT/dt values. Figure 8 shows variation in rates of temperature change over the course of a sunrise on a generic body at 1 AU when varying day length to control sunrise duration. The relative speed of the sun with respect to the horizon determines what fraction of the solar disk is exposed each moment. With the angular size of the Sun fixed, bodies with short solar days experience fast sunrises, where each moment a larger fraction of the disk begins contributing solar flux to the surface. Bodies with slow sunrises have surfaces that only get small increases in solar flux with time and thus do not produce dramatic rates of temperature change. The most extreme slowly rotating body would experience a sunrise as a quasistatic process. This difference has a greater effect on heating rates because, while the sun disappearing quickly makes the surface cool more quickly, the rate of cooling is still limited by its actual temperature, and ability to emit thermal radiation. This example also shows that the peak dT/dt value does not occur immediately when the solar flux hits the surface, but rather occurs near when half of the solar disk has been exposed. Before that point, solar flux increases at an accelerating rate. After half the disk is exposed, solar flux continues to increase, but at a slower and slower rate, driving dT/dt rates down. Finally when the solar disk is completely above the horizon, the surface gets a quasi-constant value of solar flux each moment, bringing dT/dt values down close to zero.

4. Conclusion

[26] In the model runs for surfaces on the Moon and Mercury, the highest magnitude shocks are well below the canonical threshold of 2 K/min, though surfaces on Vesta may exceed it. The uncertainty in this threshold value, however, precludes any statements about whether or not thermal stress fracturing may or may not be occurring. However, our results can still be used to get a sense of the relative efficacy of this process on various surfaces.

[27] Sunrise and sunset durations are the primary control on shock strength. The strength of shocks related to sunrise/set decreases significantly on surfaces closer to the poles due to oblique sunrises/sets taking longer at those latitudes.

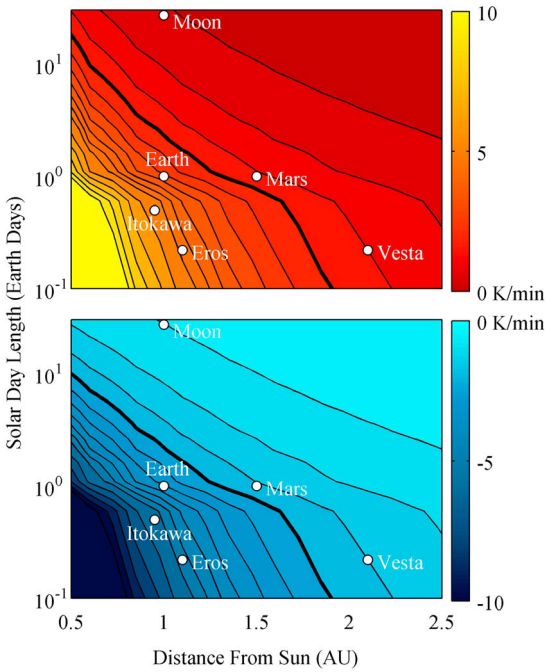

Figure 7. (top) A contour plot of dT/dt for the strongest hot (compressional) shocks as a function of body distance to the sun and solar day length on an east-facing, equatorial surface with a slope of 65°. Contour lines 0.5 K/min apart for contours ≤5 K/min, and 1 K/min between 5 K/min and 10 K/min. There is a single contour field for everything greater than 10 K/min. The bold line is the 2 K/min contour line. (bottom) The same for the strongest cold (tensional) shocks, with the bold line being −2 K/min. As in Figure 1, note that the values indicated by the Earth and Mars markers are only representative of a body with the same solar distance and rotation rate but no atmosphere.

Daytime shadowing, where the duration of the artificial sunset is independent of latitude, shows slightly higher peak dT/dt values than natural sunrise/set and no latitude dependence. In most cases, hot shocks are stronger than cold shocks although they may not necessarily cause more damage.

[28] Model runs for all bodies considering only natural sunrise/set show that the strongest shocks are experienced by highly sloped east- or west-facing surfaces. Specifically, strong hot shocks are recorded on east-facing surfaces caused by the sun rising, and cold shocks on west-facing surfaces caused by the sun setting. This suggests that overall surface breakdown and regolith production caused by thermal stress weathering should occur with an E-W distribution at the landscape scale.

[29] Model runs for all bodies considering shocks from daytime shadowing show that surfaces that experience peak dT/dts range from low to highly sloped. This is a result of the time at which the shadow is emplaced. Shadows have the strongest effect on slopes that receive the most solar flux at the time of shadowing. Thus at the equator, the strongest shocks from a shadow close to noon are seen on lower slopes because they have a smaller solar incidence angle than vertical slopes. The closer to sunrise or sunset the shadow is emplaced, the more highly sloped the surface with peak dT/dt values will be. Similarly, on surfaces closer to the poles, higher slopes receive peak shocks because the sun moves across the sky at a lower altitude. This effect also changes the aspect angle of the surfaces with the strongest shocks at higher latitudes. At the equator, peak shocks still occur on surfaces facing directly east and west, for hot and cold shocks, respectively. However, as you move higher in latitude (e.g., in the northern hemisphere) and the sun appears to be south of the surface, the aspect angles that receive the peak solar flux shift to face southeast and southwest, for hot and cold shocks, respectively.

[30] As mentioned above, shocks that occur due to daytime shadowing generally have no latitude dependence and are slightly stronger than those due to equatorial sunrises/sets. The exception to this is that hot shocks that occur during sunrise on Mercury will always be stronger than those from short-term shadowing. Bodies with long solar days cool to low temperatures at night, enabling their surfaces to heat quickly when the sun rises. Surfaces cool rapidly as the sun sets as well, but the effect is offset by heat conducted from the subsurface. This appears to be true regardless of whether they were caused by the natural sunrise/set or daytime shadowing. In general, for slowly rotating bodies, the shorter their distance to the sun the stronger their hot shocks will be, and the greater difference there will be between the strengths of hot and cold shocks (though in most cases shocks from morning and afternoon shadows are roughly equivalent in strength).

[31] Vesta experiences more rapid changes in temperature than the Moon and Mercury due to the fact that its sunrises/sets are rapid. Seasonal effects on solar distance (influencing flux) and sub-solar latitude mean peak shocks are the result of oblique sunrises/sets even at the equator. Daytime shadowing (assumed to be horizon normal) thus produces much stronger

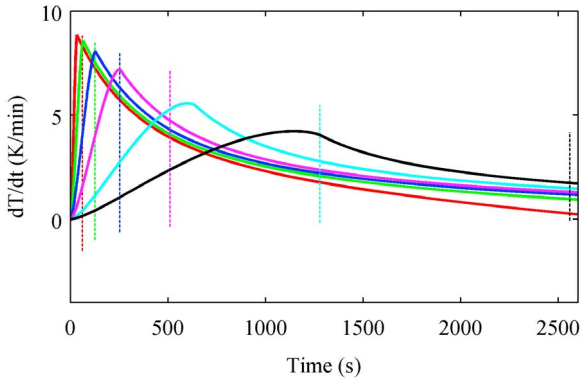

Figure 8. Rates of temperature change over the course of one sunrise on a generic body at 1 AU and varying day length. The line with highest dT/dt value corresponds to the body with the shortest day and fastest sunrise. The day lengths, from shortest to longest, are 0.25, 0.5, 1, 2, 5, and 10 Earth days, corresponding to sunrise durations of 62, 126, 254, 510, 1278, and 2558 s, respectively. The dotted lines mark the end of the sunrises, when the solar disk is fully above the horizon, in each case. Each line is normalized to begin at the same point on the *x* axis.

shocks than natural sunrises/sets, even at the equator, with values exceeding the canonical threshold. Hot and cold shocks produced by morning shadowing are comparable in value, as are hot and cold shocks produced by afternoon shadowing.

[32] The presence of high dT/dt values does not necessarily indicate high dT/dz values. Of each of the three bodies tested, Mercury experienced the strongest spatial temperature gradients, followed by the moon. Vesta experienced the strongest dT/dt, but the weakest dT/dz. This is a consequence of the relatively low surface temperatures that result from its short solar day length and distance from the sun. On a warmer body like the Moon or Mercury, the change in temperature that occurs during sunrise or sunset causes a large spatial temperature gradient to be established because the surface is radiating heat away much faster than the subsurface layers can supply it. On Vesta, however, even during periods yielding rapid rates of temperature change, conduction of heat within the subsurface has comparable efficiency to loss of heat through radiation emitted at the colder surface, thus a large thermal gradient is never set up. The lack of correlation between dT/dt and dT/dz emphasizes that thermal damage may vary significantly with environment, not just with rock properties, underlining the need for further research to understand the thermal stress weathering process.

[33] While we can determine which surfaces on a given body may be most susceptible to the thermal stress weathering process, we cannot say with any certainty whether or not the process competes effectively with other surface modification processes (e.g., from micrometeorite bombardment). The rise in dT/dt values with decreasing distance to the sun and/or solar day length suggests that thermal stress weathering may be more effective on certain bodies; however, the relationship between macroscopic temporal and spatial temperature gradients and the threshold for microscopic fractures to form is still unknown. In reality, the threshold will vary with rock type, size, and amount of pre-existing damage [*Bahr et al.*, 1986; *Weiss et al.*, 2003]. It will also vary with the scale of the induced temperature gradient. At scales larger than the characteristic crack length of the rock, shocks will serve to propagate pre-existing cracks. At smaller scales, however, a larger shock will be required to initiate a new crack. Much more work needs to be done in order to understand the implications of this relationship on the efficacy of thermal stress weathering in the solar system.

Appendix A

A1. Model Approximations

[34] Highly sloped surfaces have very different temperatures than flat surfaces at a given time of day. To include properly the effect of this temperature difference, equation (9) would be replaced by:

$$L = \varepsilon\sigma T_{slope}^4 - \sin^2\left(\frac{\theta}{2}\right)\varepsilon^2\sigma T_{flat}^4 \qquad \text{(A1)}$$

We chose to simplify this term by assuming that the surface is surrounded by an infinite flat plane of the same temperature ($T_f \cong T_s$) and that $\varepsilon \cong \varepsilon^2$. However, slopes stay warmer at night so using equation (A1) makes surrounding flat terrain colder. This effect lowers rates of temperature change during sunrise because surrounding terrain then contributes less radiation to the slope as it warms up. During sunset, the warmth of the flat terrain slightly decreases the cooling rate of a highly sloped surface, as it will provide a source of flux even after the surface has become shaded. To test the importance of this effect, we compared model runs using equation (9) and (A1). We tested surfaces with the two highest dT/dt-producing optimal geometries on Mercury, with slopes of 90° and aspect angels of 90° and 270°. These cases are ideal, as they will have the largest temperature difference between flat and sloped ground of any surfaces, on any body. Using equation (A1) instead of (9) lowers the peak dT/dt value by 8.4% and 5.1% during sunrise and sunset, respectively. These values do not represent a significant change to our results, especially given the lack of understanding of any damage threshold, and at what resolution it may exist. Therefore, we have opted to use the simpler method of accounting for radiation from surrounding terrain (i.e., equation (9)). Note that tests in the following sections were also done using one or both optimal geometries.

A2. Shadowing and the Solar Disk

[35] It was important to account for the size of the solar disk during sunrise and sunset events, as assuming the sun as a point source yields extremely high, unphysical rates of temperature change. For natural sunrises/sets, we did this by scaling the incident solar flux linearly with the area of the visible portion of the solar disk. The incidence vector was adjusted to intersect the center of whatever portion of the disk was above the horizon for each time step. In cases where we introduced artificial shadows during the day, it was necessary to simplify the approximation further. Because the shadows were placed at arbitrary times during the insolation cycle, the obliqueness of the artificial sunrises/sets were also arbitrary. In these cases, we accounted for the size of the solar disk during artificial sunrise by scaling the incident solar flux linearly from zero to its value when the disk just cleared the local horizon with the amount of time it took for this to occur, and vice versa for artificial sunsets. For the Moon and Mercury, the length of time it took for this to occur was calculated for the day on which each model run took place. For Vesta, each model run is calculated on the day during Vesta's orbit that produces peak dT/dt values for that set of parameter values. However, all of these days occur close to perihelion, and so only a single calculation was made (at perihelion) for the length of time of sunrises/sets in artificial shadows.

[36] The artificial shadows were introduced during the same times relative to the solar day in the morning and afternoon on each body, though with different durations. The length of time for which the surface was shadowed was on the order of hours for the Moon, tens of hours for Mercury, and minutes for Vesta. The shadow duration has an affect on both the heating and the cooling rate of the surface. During a sunset, the cooling rate increases until the disk is fully below the horizon. In the example from Figure 2 for Mercury, it takes approximately 11 h for this to occur, and perhaps another 10 for dT/dt values to return to close to zero (Figure A1). Thus if the shadow is shorter than 11 h, then the surface has not reached its peak dT/dt value yet. We chose shadows longer than this sunset

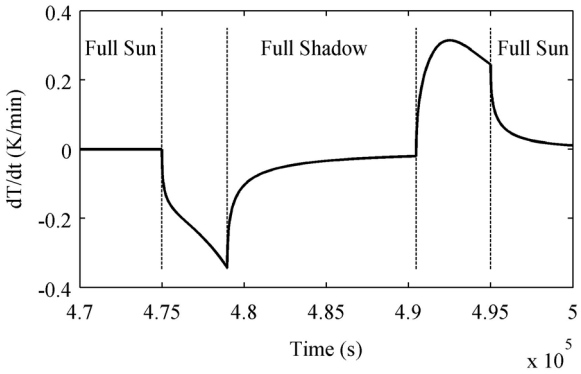

Figure A1. Rate of surface temperature change caused by an artificial shadow imposed on the Mercurian surface described in Figure 2. This figure demonstrates the effect of shadow duration, as well as the difference between heating and cooling behavior, on the surface.

time on each body to avoid complications and to record maximum possible dT/dt values. During a sunrise, it is the surface temperature the affects the heating rate. The longer the surface is in shadow, the cooler it becomes, and thus the more dramatic heating rates will occur. This becomes a significant effect when the shadows begin to approach timescales on the order of the duration of the body's night. None of our shadows emplaced long enough to compete with heating rates that occur during natural sunrise.

A3. Variation of Thermophysical Parameters

[37] To investigate how much variation in surface properties may affect thermal stress weathering we tested the sensitivity of the results to each parameter: albedo, emissivity, density, heat capacity, and thermal conductivity. In each test, all parameters were held at their constant, baseline value for bedrock except one, which was varied over some range. The baseline values and range tested for each parameter are shown in Table A1. Density and heat capacity were tested as a product and not as individual parameters. Results of sensitivity tests, also shown in Table A1, are for the lunar surface. Tests for Mercury did not differ significantly. Three latitudes were tested, with every combination of slope and aspect angle as discussed in the previous section. For conciseness, only peak dT/dt values over equatorial surfaces experiencing positive changes in temperature (hot shocks) are shown in the table, as this case was the most sensitive to changes in thermophysical parameter values.

[38] In general, increasing any of the parameters resulted in a decrease in magnitude of dT/dt values. This occurs because the increase either decreases the net amount of energy the surface absorbs or increases its ability to conduct energy into the subsurface. The decrease in magnitude of dT/dt is very small (typically <0.05 K/min) for the albedo, emissivity, and density*heat capacity. Varying the thermal conductivity had the largest affect on the model results.

[39] To determine the total range of dT/dt values we compared results of a model run using the lowest value in each parameter's range, to produce the hottest surface, to a run using the highest parameter values, producing the coolest surface. Since the variation is primarily controlled by the thermal conductivity, the sensitivities in these cases are comparable to the previously mentioned baseline cases where only k is varied. When changing from low to high parameter values, the magnitude of dT/dt values decreased by 0.569 K/min. While this test shows that parameter values can influence rates of temperature change by up to a factor of two, it is difficult to relate this to uncertainty in thermal damage.

A4. Variation of Model Resolution and Initial Conditions

[40] The Moon and Mercury have minimum sunrise/set durations of ~1 h, ~8 h. For these cases we used a constant model time step of 10 s. These models were tested at smaller times steps to be sure that the solution converged. Vesta has a much shorter sunrise/set duration of ~12, requiring smaller model resolution. In these cases we used a time step of 0.01 s. We also tested this time step to be sure our results converged.

[41] The duration of sunrises/sets determine what thickness of model layers has sufficient resolution. In our model for the Moon and Mercury, the first 10 layers are 0.005 m thick and the subsequent layers follow the relationship $dz_i = 1.03*dz_{i-1}$. This is appropriate, as the skin depths of sunrises/sets on each body is ~0.08 and ~0.03 m, respectively. Given 120 layers, this relationship gives a maximum depth of ~4.5 m. This is multiple skin depths on each body for a daily cycle, and most importantly for the sunrise/set duration, but not for a yearly cycle. We ran the optimal geometry cases on each body with a function $dz_i = 1.05*dz_{i-1}$, resulting in a maximum depth of ~24 m. Increasing the model depth produces maximum changes in surface dT/dt of 0.3% for both hot and cold shocks on the Moon, and of 1% and 0.1%, respectively, on Mercury.

[42] Vesta's sunrise/set has a much smaller skin depth (~0.002 m) so we chose a thickness of 0.0005 m with subsequent layers following the relationship $dz_i = 1.04*dz_{i-1}$. This gives a maximum depth of ~1 m, which is appropriately thick for the length of day and sunrise/set durations on

Table A1. Results of Sensitivity Test Values Used for Each Model Parameter During the Sensitivity Study, and the Effect of Each Parameter on dT/dt Values[a]

				ΔdT/dt (K/min)	
Parameter	Low	Baseline	High	Low	High
Albedo	0.04	0.1	0.16	0.039	−0.039
ε	0.8	0.9	1	4E-4	−4E-4
$\rho*c_p$ (kg/m^3)	2E6	2.4E6	3E6	0.055	−0.061
k (J/m K)	1	2	3	0.243	−0.108
Max dT/dt	0.978	0.597	0.409		

[a]The values chosen were gathered from the literature [*Robertson*, 1988; *Mellon et al.*, 2008; *Bandfield et al.*, 2011; *Turcotte and Schubert*, 2002]. The sample model run is for an equatorial surface on the Moon experiencing positive changes in temperature (hot shocks). The two rightmost columns show the change in peak dT/dt value for each model run when a single parameter is either decreased or increased from the baseline value. The bottom row shows the peak dT/dt value for the baseline model run, and when all parameters are either decreased or increased at the same time (the optimal and non-optimal cases). These tests cover a total range of thermal inertia values from 1549–2683 J/m^2 Ks$^{1/2}$.

Vesta. It is smaller than necessary for the yearly cycle, however tests to find the days producing the highest dT/dt values at various latitudes indicate that all peak days occur near perihelion, in both the northern and southern hemispheres. For this reason, and those discussed below, we determined that seasonal effects were not relevant in this context.

[43] Before collecting data, each model run was initialized by setting a reasonable surface temperature and making the gradient linear with depth. The surface temperatures and temperatures at depth were chosen based on the results of *Vasavada et al.* [1999]. The model was then run for several days until the daily temperatures repeated themselves. In the case of Mercury, several insolation cycles is the equivalent of several years, and thus the model achieved annual temperature repetition. The Moon was not equilibrated over a period of multiple years as is often done with this type of modeling. Since the Moon has such a small obliquity and eccentricity, and no relevant surface processes (e.g., frost action), we determined seasonal effects in our model runs to be negligible. In general, while seasonal effects can influence surface and subsurface temperatures, they have very little impact on rates of surface temperature change.

[44] Vesta is a slightly more complicated body and the small time step makes it inefficient to run over long time periods. To simplify the model computationally, we ran the model at a very low resolution for several Vesta years to find the annual average surface temperature at each latitude. These temperatures were used as initial values for the higher resolution model runs. Then the model was run on the surface's peak day for several iterations before collecting data in order to normalize the temperature values. To ensure the initial conditions had no effect on our results, we ran the model for one surface (which had an optimal geometry) over a period of 6 Vesta years, at a time step of 21 s, and with a total model depth of 26 m. Comparing these results to those that were only run for a few days found that the magnitude of dT/dt values changed by only 1.5%.

References

Acton, C. H. (1996), Ancillary data services of NASA's Navigation and Ancillary Information Facility, *Planet. Space Sci.*, *44*, 65–70, doi:10.1016/0032-0633(95)00107-7.

Bahr, H. A., G. Fischer, and H. J. Weiss (1986), Thermal-shock crack patterns explained by single and multiple crack propagation, *J. Mater. Sci.*, *21*, 2716–2720, doi:10.1007/BF00551478.

Bandfield, J. L., R. R. Ghent, A. R. Vasavada, D. A. Paige, S. J. Lawrence, and M. S. Robinson (2011), Lunar surface rock abundance and regolith fines temperatures derived from LRO Diviner Radiometer data, *J. Geophys. Res.*, *116*, E00H02, doi:10.1029/2011JE003866.

Blackwelder, E. (1933), The insolation hypothesis of rock weathering, *Am. J. Sci.*, *26*, 97–113, doi:10.2475/ajs.s5-26.152.97.

Cooke, R. U., and I. J. Smalley (1968), Salt weathering in deserts, *Nature*, *220*, 1226–1227, doi:10.1038/2201226a0.

Dombard, A. J., O. S. Barnouin, L. M. Prockter, and P. C. Thomas (2010), Boulders and ponds on the Asteroid 433 Eros, *Icarus*, *210*, 713–721, doi:10.1016/j.icarus.2010.07.006.

Eppes, M. C., and D. Griffing (2010), Granular disintegration of marble in nature: A thermal-mechanical origin for a grus and corestone landscape, *Geomorphology*, *117*, 170–180, doi:10.1016/j.geomorph.2009.11.028.

Eppes, M. C., L. D. McFadden, K. W. Wegmann, and L. A. Scuderi (2010), Cracks in desert pavement rocks: Further insights into mechanical weathering by directional insolation, *Geomorphology*, *123*, 97–108, doi:10.1016/j.geomorph.2010.07.003.

Gómez-Heras, M., B. J. Smith, and R. Fort (2006), Surface temperature differences between minerals in crystalline rocks: Implications for granular disaggregation of granites through thermal fatigue, *Geomorphology*, *78*, 236–249, doi:10.1016/j.geomorph.2005.12.013.

Griggs, D. T. (1936), The factor of fatigue in rock exfoliation, *J. Geol.*, *44*, 783–796, doi:10.1086/624483.

Gunzburger, Y., and V. Merrien-Soukatchoff (2011), Near-surface temperatures and heat balance of bare outcrops exposed to solar radiation, *Earth Surf. Processes Landforms*, *36*, 1577–1589, doi:10.1002/esp.2167.

Hall, K. (1997), Rock temperatures and implications for cold region weathering: I. New data from Viking Valley, Alexander Island (Antarctica), *Permafrost Periglacial Proc.*, *8*, 69–90, doi:10.1002/(SICI)1099-1530(199701)8:1<69::AID-PPP236>3.0.CO;2-Q.

Hall, K. (1998), Rock temperatures and implications for cold region weathering: II. New data from Rothera, Adelaide Island (Antarctica), *Permafrost Periglacial Proc.*, *9*, 47–55, doi:10.1002/(SICI)1099-1530(199801/03)9:1<47::AID-PPP273>3.0.CO;2-N.

Hall, K. (1999), The role of thermal stress fatigue in the breakdown of rock in cold regions, *Geomorphology*, *31*, 47–63, doi:10.1016/S0169-555X(99)00072-0.

Hall, K., and M. F. Andre (2001), New insights into rock weathering from high-frequency rock temperature data: An Antarctic study of weathering by thermal stress, *Geomorphology*, *41*, 23–35, doi:10.1016/S0169-555X(01)00101-5.

Hall, K., and M. F. Andre (2003), Rock thermal data at the grain scale: Applicability to granular disintegration in cold environments, *Earth Surf. Processes Landforms*, *28*, 823–836, doi:10.1002/esp.494.

Hallet, B. (2006), Why do freezing rocks break?, *Science*, *314*, 1092–1093, doi:10.1126/science.1135200.

Jansen, D. P., S. R. Carlson, R. P. Young, and D. A. Hutchins (1993), Ultrasonic imaging and acoustic emission monitoring of thermally induced microcracks in Lac du Bonnet granite, *J. Geophys. Res.*, *98*, 22,231–22,243, doi:10.1029/93JB01816.

Koch, A., and S. Siegesmund (2004), The combined effect of moisture and temperature on the anomalous expansion behaviour of marble, *Environ. Geol.*, *46*, 350–363.

Lu, J., and N. A. Fleck (1998), The thermal shock resistance of solids, *Acta Mater.*, *46*, 4755–4768, doi:10.1016/S1359-6454(98)00127-X.

Luque, A., E. Ruiz-Agudo, G. Cultrone, E. Sebastian, and S. Siegesmund (2011), Direct observation of microcrack development in marble caused by thermal weathering, *Environ. Earth Sci.*, *62*, 1375–1386, doi:10.1007/s12665-010-0624-1.

McFadden, L. D., M. C. Eppes, A. R. Gillespie, and B. Hallet (2005), Physical weathering in arid landscapes due to diurnal variation in the direction of solar heating, *Geol. Soc. Am. Bull.*, *117*, 161–173, doi:10.1130/B25508.1.

McKay, C. P., J. L. Molaro, and M. M. Marinova (2009), High-frequency rock temperature data from hyper-arid desert environments in the Atacama and the Antarctic Dry Valleys and implications for rock weathering, *Geomorphology*, *110*, 182–187, doi:10.1016/j.geomorph.2009.04.005.

Mellon, M. T., R. L. Fergason, and N. E. Putzig (2008), The thermal inertia of the surface of Mars, in *The Martian Surface: Composition, Mineralogy and Physical Properties*, edited by J. Bell, pp. 399–427, Cambridge Univ. Press, Cambridge, U. K.

Molaro, J. L., and C. P. McKay (2010), Processes controlling rapid temperature variations on rock surfaces, *Earth Surf. Processes Landforms*, *35*, 501–507.

Moores, J. E., J. D. Pelletier, and P. H. Smith (2008), Crack propagation by differential insolation on desert clasts, *Geomorphology*, *102*, 472–481, doi:10.1016/j.geomorph.2008.05.012.

Richter, D., and G. Simmons (1974), Thermal expansion behavior of igneous rocks, *Int. J. Rock Mechanics*, *11*, 403–411, doi:10.1016/0148-9062(74)91111-5.

Robertson, E. C. (1988), Thermal properties of rocks, *U.S. Geol. Surv. Open File Rep.*, *88–441*, 110 pp.

Siegesmund, S., J. Ruedrich, and A. Koch (2008), Marble bowing: Comparative studies of three different public building facades, *Environ. Geol.*, *56*, 473–494.

Sumner, P. D., K. I. Meiklejohn, W. Nel, and D. W. Hedding (2004), Thermal attributes of rock weathering: Zonal or azonal? A comparison of rock temperatures in different environments, *Polar Geogr.*, *28*, 79–92, doi:10.1080/789610119.

Sumner, P. D., D. W. Hedding, K. I. Meiklejohn (2007), Rock surface temperatures in southern Namib and implications for thermally driven physical weathering, *Z. Geomorphol.*, *51*, supplement, 133–147.

Turcotte, D. L., and G. Schubert (2002), *Geodynamics*, Cambridge Univ. Press, New York.

Vasavada, A. R., D. A. Paige, and S. E. Wood (1999), Near-surface temperatures on Mercury and the Moon and the stability of polar ice deposits, *Icarus*, *141*, 179–193, doi:10.1006/icar.1999.6175.

Viles, H. A. (2005), Microclimate and weathering in the central Namib Desert, *Geomorphology*, *67*, 189–209, doi:10.1016/j.geomorph.2004.04.006.

Viles, H. A., B. Ehlmann, C. F. Wilson, T. Cebula, M. Page, and M. Bourke (2010), Simulating weathering of basalt on Mars and Earth by thermal cycling, *Geophys. Res. Lett.*, *37*, L18201, doi:10.1029/2010GL043522.

Weiss, T., S. Siegesmund, and E. R. Fuller Jr. (2003), Thermal degradation of marble: Indications from finite-element modeling, *Build. Environ.*, *38*, 1251–1260, doi:10.1016/S0360-1323(03)00082-9.

Wellman, H. W., and A. T. Wilson (1965), Salt weathering: A neglected geological erosive agent in coastal arid environments, *Nature*, *205*, 1097–1098, doi:10.1038/2051097a0.